REPORT DOCUMENTATION PAGE

Form Approved

OMB No. 0704-0188

1. REPORT DATE *(DD-MM-YYYY)*	2. REPORT TYPE	3. DATES COVERED *(From - To)*
09-02-2015	Final	20120926- 20140925

4. TITLE AND SUBTITLE

High Rate Performing Lithium Ion Battery

5a. CONTRACT NUMBER
FA2386-12-1-4085

5b. GRANT NUMBER
Grant AOARD-124085

5c. PROGRAM ELEMENT NUMBER
61102F

6. AUTHOR(S)

Prof. Palani Balaya

5d. PROJECT NUMBER

5e. TASK NUMBER

5f. WORK UNIT NUMBER

7. PERFORMING ORGANIZATION NAME(S) AND ADDRESS(ES)

NATIONAL UNIVERSITY OF SINGAPORE
21 LOWER KENT RIDGE ROAD
SINGAPORE 119077

8. PERFORMING ORGANIZATION REPORT NUMBER

N/A

9. SPONSORING/MONITORING AGENCY NAME(S) AND ADDRESS(ES)

AOARD
UNIT 45002
APO AP 96338-5002

10. SPONSOR/MONITOR'S ACRONYM(S)

AFRL/AFOSR/IOA(AOARD)

11. SPONSOR/MONITOR'S REPORT NUMBER(S)

AOARD-124085

12. DISTRIBUTION/AVAILABILITY STATEMENT

Distribution Code A: Approved for public release, distribution is unlimited.

13. SUPPLEMENTARY NOTES

14. ABSTRACT To reduce charging time, an integrated power storage device of of batteries and supercapacitors in one unit is proposed. The novel energy storage device will have relatively high energy density comparable to batteries as well as high power density as that of supercapacitors. Potential materials for such a supercap battery are Li3V2(PO4)3 (LVP) and LiNi1/3Mn1/3CO1/3O2 (NMC) as cathodes and titanium-based Li4Ti5O12 (LTO) as anode respectively to provide high storage capacity and high rate performance.
A detailed investigation on LVP cathode demonstrated that both the high rate performance and long term cyclability of LVP can be improved by preparing electrode material with a favourable architecture. Phenomenological studies were also conducted, as was preliminary work toward scaling components into a full-size power storage unit. Further work is underway to increase the energy density to 90 Wh/kg using alternative cathode materials.

15. SUBJECT TERMS

NDE, Finite Difference Methods, Carbon Fiber composites

16. SECURITY CLASSIFICATION OF:			17. LIMITATION OF ABSTRACT	18. NUMBER OF PAGES	19a. NAME OF RESPONSIBLE PERSON
a. REPORT	b. ABSTRACT	c. THIS PAGE			David Hopper, Lt Col, USAF, Ph.D.
U	U	U	SAR	22	19b. TELEPHONE NUMBER *(Include area code)* +81-42-511-2000

Report Documentation Page

Form Approved
OMB No. 0704-0188

1. REPORT DATE	2. REPORT TYPE	3. DATES COVERED
26 MAR 2015	**Final**	**26-09-2012 to 25-09-2014**

4. TITLE AND SUBTITLE	5a. CONTRACT NUMBER
High Rate Performing Lithium Ion Battery	**FA2386-12-1-4085**
	5b. GRANT NUMBER
	5c. PROGRAM ELEMENT NUMBER **61102F**

6. AUTHOR(S)	5d. PROJECT NUMBER
Palani Balaya	5e. TASK NUMBER
	5f. WORK UNIT NUMBER

7. PERFORMING ORGANIZATION NAME(S) AND ADDRESS(ES)	8. PERFORMING ORGANIZATION REPORT NUMBER
NATIONAL UNIVERSITY OF SINGAPORE,21 LOWER KENT RIDGE ROAD,SINGAPORE ,119077,NA,NA	**N/A**

9. SPONSORING/MONITORING AGENCY NAME(S) AND ADDRESS(ES)	10. SPONSOR/MONITOR'S ACRONYM(S)
AOARD, UNIT 45002, APO, AP, 96338-5002	**AFRL/AFOSR/IOA(AOARD)**
	11. SPONSOR/MONITOR'S REPORT NUMBER(S) **AOARD-124085**

12. DISTRIBUTION/AVAILABILITY STATEMENT
Approved for public release; distribution unlimited

13. SUPPLEMENTARY NOTES

14. ABSTRACT
To reduce charging time, an integrated power storage device of of batteries and supercapacitors in one unit is proposed. The novel energy storage device will have relatively high energy density comparable to batteries as well as high power density as that of supercapacitors. Potential materials for such a supercap battery are Li3V2(PO4)3 (LVP) and LiNi1/3Mn1/3CO1/3O2 (NMC) as cathodes and titanium-based Li4Ti5O12 (LTO) as anode respectively to provide high storage capacity and high rate performance. A detailed investigation on LVP cathode demonstrated that both the high rate performance and long term cyclability of LVP can be improved by preparing electrode material with a favourable architecture. Phenomenological studies were also conducted, as was preliminary work toward scaling components into a full-size power storage unit. Further work is underway to increase the energy density to 90 Wh/kg using alternative cathode materials.

15. SUBJECT TERMS
NDE, Finite Difference Methods, Carbon Fiber composites

16. SECURITY CLASSIFICATION OF:			17. LIMITATION OF ABSTRACT	18. NUMBER OF PAGES	19a. NAME OF RESPONSIBLE PERSON
a. REPORT	b. ABSTRACT	c. THIS PAGE			
unclassified	**unclassified**	**unclassified**	**Same as Report (SAR)**	**22**	

Final Report for AOARD Grant FA2386-12-1-4085

"High Rate Performing Li-ion Battery"

09 Feb. 2015

Name of Principal Investigators (PI): A/Prof. Palani Balaya

- e-mail address : mpepb@nus.edu.sg
- Institution : National University of Singapore
- Mailing Address:
  Dr. Palani Balaya
  Associate Professor
  Department of Mechanical Engineering, Faculty of Engineering,
  National University of Singapore,
  SINGAPORE 117576
- Phone : 0065-62768177
- Fax : 0065-67791459

Period of Performance: Sept./26/2012 – Sept. /25/2014

Abstract

The major concern about the existing rechargeable Li-ion battery technology for military applications is that it takes too long time for recharging. Current proposal aims to provide a battery technology solution for defense applications with all the advantages of batteries and supercapacitors in one unit. In other words, the novel energy storage device will have relatively high energy density comparable to batteries as well as high power density as that of supercapacitors. Potential materials for such a supercap battery are $Li_3V_2(PO_4)_3$ (LVP) and $LiNi_{1/3}Mn_{1/3}CO_{1/3}O_2$ (NMC) as cathodes and titanium-based $Li_4Ti_5O_{12}$ (LTO) as anode respectively to provide high storage capacity and high rate performance.

In this study, we did a detailed investigation on LVP cathode and demonstrated that both the high rate performance and long term cyclability of LVP can be improved by preparing electrode material with a favourable architecture. We also attempted to address the cause for the observed exceptional high rate performance in LVP. For the first time we have reported electron spin resonance experiment down to 10K on LVP to discuss valance states of transition metal ions upon lithium extraction and insertion. We also investigated storage mechanism using X-ray diffraction experiment restricting the voltage windows for lithium storage.

As part of developing novel 18650 cells with new electrode chemistry, LVP cathode material has been scaled up successfully up to 50 g in one pot. The electrochemical performance was evaluated in each stage (5, 25 and 50 g) of scaling up process using coin cells. LTO anode material has also been scaled up systematically from 25 to 100g using one pot synthesis approach and its electrochemical performance was evaluated in each batch. Commercial type lithium-ion battery (18650) cells were fabricated using in-house pilot line with the above LTO anode along with commercial NMC cathode material with an energy density of 63 Wh/kg which shows comparable storage performance as commercial batteries. Further work is in progress in order to increase the energy density to about 90 Wh/kg using alternative cathode materials.

A. Introduction

(i) Fundamental contributions

The phosphate framework materials $LiMPO_4$ (M= Co, Ni, Mn)[1-8] and $Li_3M_2(PO_4)_3$ (M = Fe, and V)

[9,10] have been investigated extensively as the potential alternate for $LiCoO_2$ cathode material. This is because these materials can exhibit better structural stability, competitive energy and power density as compared to unstable $LiCoO_2$. Among these phosphate materials, monoclinic α-$Li_3V_2(PO_4)_3$ (LVP) has received considerable attention as a prospective cathode material due to its high storage capacity (197 $mAhg^{-1}$ vs. Li/Li^+) [10-15]. Notably, this storage capacity is known so far the highest among all phosphate-based cathode materials. Unlike olivine $LiFePO_4$ with inherent low lithium ion diffusion dimensionality [16,17] and poor lithium ion diffusion (10^{-14}-10^{-16} cm^2s^{-1}) [18], the NASICON structured LVP with space group $P2_1/n$ comprises of a three dimensional framework of metal octahedral (VO_6) and phosphate tetrahedral (PO_4) sharing oxygen vertices (**Figure 1**) [19-21] which enables lithium ions transport in three dimensional pathways [22,23], resulting in relatively higher lithium ion diffusion ($\sim10^{-9}$-10^{-10} cm^2s^{-1}).[24] However, similar to $LiFePO_4$, the main drawback of LVP is its intrinsic poor electronic conductivity (10^{-8} Scm^{-1}) [25] which can hinder its applications in high power density LIBs. In this study, we have demonstrated that the high rate performance and long term cyclability can be improved by preparing electrode material with a favourable architecture. The tailored carbon coated LVP/C morphology reported here features interconnected nano-particles with mesoporous architecture, resulting in improved electrolyte-electrode wettability, reduced transport length for lithium ions and conductive wiring for facile electron transfer thus, enhancing the rate performance.

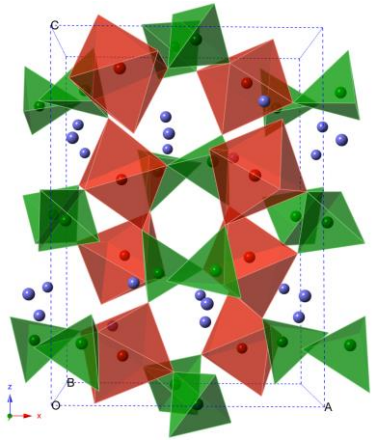

Figure 1 View of monoclinic α-$Li_3V_2(PO_4)_3$ structure on *xz* plane. Blue: Li; red: VO_6 and green: PO_4

Though LVP cathode material has been successfully developed in our group at the laboratory scale with favorable storage performances, some of the fundamental questions have not been addressed. For example, the reason for the exceptional high rate performance (90 mAh/g at 30C) is still not clear in the proposed cathode $Li_3V_2(PO_4)_3$, a NASICON structured 3-D lithium-ion conductor. We performed a systematic morphology examination, electrochemical study, ex-situ XRD and electron spin resonance (ESR) experiments to address above questions. We reported electrochemical performance of tailored LVP/C with different voltage windows, delivering differential capacity and voltage profiles with respect to the site potential of the lithium and interaction with $V^{3+}/V^{4+}/V^{5+}$ redox couples in the lattice structure. Reversible extraction/insertion electrochemical process has been confirmed by ex-situ XRD patterns recorded at various stages of charging and discharging cycle. Further, ESR spectra provided valuable information about possible changes in the local coordination of vanadium ions and their valence state during extraction and insertion of lithium ions into the host matrix of vanadium phosphate.

(ii) Fabrication of commercial type Li-ion battery

Combining phosphates with conventional graphitic anodes in a full-cell poses serious limitations to the subsequent safety of the system. Especially, at high current rates, the possibility of lithium plating is high owing to the very low intercalation potential of lithium in graphite (~ 200 mV vs. Li/Li^+). Such plated lithium grow further into dendrites which tear the separator apart leading to internal shorting and a potential thermal runaway (**Figure 2**).[26] Hence from a safety standpoint the choice of an

appropriate anode material becomes extremely crucial for high power applications. Besides safety, the ability of batteries to be rapidly charged/ discharged is also an important requisite of energy storage systems. However, in most cases, rapid charge/discharge process is accompanied by drastic reduction in the delivered capacities, leading to lower energy densities. Hence, anode materials that combine rapid charge/discharge with excellent capacity retention are required.

In view of the above requirements, $Li_4Ti_5O_{12}$ (LTO) has been considered to be an ideal candidate for high power applications owing to the following reasons namely (a) stable cycle life - no significant unit cell volume change during Li insertion/extraction[27,28] (b) better safety - a high plateau potential at 1.55 V vs. Li/Li^+ eliminating the possibility of lithium dendrite formation[29,30] and (c) low irreversible capacity loss - the operating voltage of LTO is higher than the potential at which SEI layer formation happens. Hence, all these features have favored LTO for use in commercial applications.[31]

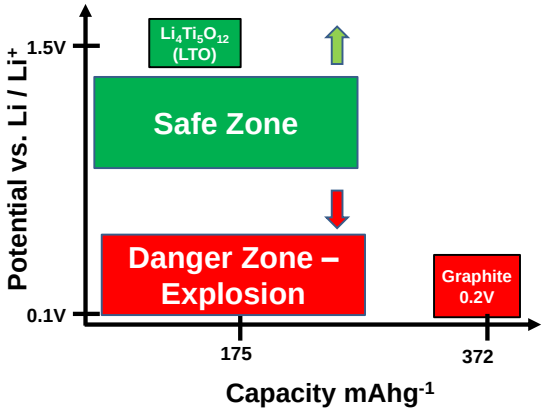

Figure 2 $Li_4Ti_5O_{12}$ for ultrafast charge-discharge with safe operating voltage window

LTO belongs to the $Fd\bar{3}m$ space group with a cubic spinel structure where, lithium and titanium ions occupy the tetrahedral *8(a)* and octahedral *16(d)* sites respectively (**Figure 3**). Oxygen ions are reported to be located on the *32(e)* sites to form a three-dimensional edge sharing octahedral structure $[Li_{1/6}Ti_{5/6}]O_6$.[27]

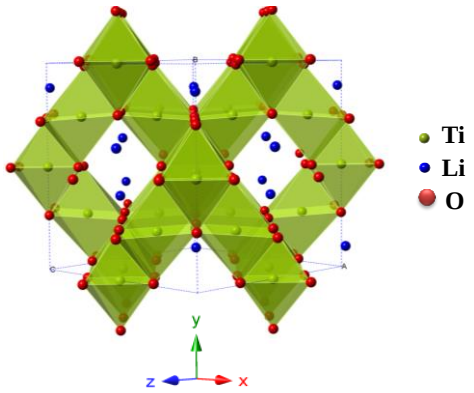

Figure 3 Spinel structure of $Li_4Ti_5O_{12}$

We scaled up production of above materials, $Li_3V_2(PO_4)_3$ as well as titanate based anode (LTO), in order to fabricate novel military grade Li-ion battery (18650 cells) using the battery pilot line at NUS. As an initial step, LVP cathode material was scaled up successfully up to 50 g using one pot synthesis approach. The electrochemical performance was evaluated in each stage (5, 25 and 50 g) of scaling up process using coin cells against lithium metal (half-cell).

LTO anode material has been developed successfully up to 100g of material in one pot. This material was scaled up systematically from 5 to 25 to 100g; electrochemical performance was evaluated in each batch of material.

18650 cells were also fabricated using in-house scaled up LTO and commercial NMC cathode material. This battery upon several optimization resulted in an energy density of 63 Wh/kg which is comparable or even slightly higher than the commercial LTO-based batteries.

B. Experiment

(i) $Li_3V_2(PO_4)_3$ synthesis and material characterization

All chemical precursors and solvents are commercially available and used as received without further purification. 0.01M of cetyl trimethylammonium bromide (CTAB) surfactant was dissolved in ethanol solution. The starting materials, lithium acetate hydrate ($LiOOCCH_3.H_2O$), vanadium (IV) oxide bis(2,4-pentanadionate) ($C_{10}H_{14}O_5V$) and ammonium dihydrogen phosphate ($(NH_4)H_2PO_4$) in a stoichiometric molar ratio were added into the prepared CTAB-ethanol solution. Then, deionized water was added into the solution with ethanol-water volume ratio of 5:1. The solution was stirred for 24-60 hour (h) and dried using rotor evaporator at temperature 70 °C. After drying, the obtained powder was sintered in tube furnace under argon atmosphere at 600-800 °C for 6-12 h.

The phase of LVP/C was characterized by X-ray diffraction (XRD) 6000 SHIMADZU, Japan with Cu-K_α radiation (λ = 1.54056 Å). The morphology and microstructure of obtained powder were investigated by HITACHI S4300 field emission scanning electron microscopy (FESEM) at 15 kV and transmission electron microscopy (TEM) at 200 kV (JEOL-2010F). Resonant Raman scattering spectrum of LVP/C was recorded at room temperature using Raman spectrometer JYT6400. BET surface area was measured at 77 K on Nova 2200e surface area (Quantachrome, USA). Prior to the measurement, the sample was degassed at 130 ^oC for 12-24 h. Electron Spin Resonance technique (ESR) was used to investigate the valence states and the local coordination of vanadium ions in LVP/C. ESR measurements were carried out by means of Bruker spectrometer at a frequency 9.2 GHz (X-band) in temperature range 10-300 K. The approximation of experimental ESR spectra was performed by means of EasySpin software.

The LVP/C electrodes comprises of a mixture of active material, Super P or Denka black and polyvinylidene difluoride (PVDF) (Kynar 2801) at a weight ratio of 75:15:10/80:10:10 in N-methyl-2-pyrrolidone (NMP) solvent. Then, electrodes were prepared using an etched aluminium foil as current collector via doctor-blade technique. Electrochemical performance of electrodes were investigated using CR2016 coin-type cells. The coin cells were assembled in argon-filled glove box (MBraun, Germany). Whatman binder-free glass microfiber filter (type GF/F) was used as the separator, lithium metal foil was used as the anode, and 1-M lithium hexafluorophosphate ($LiPF_6$) in ethylene carbonate/diethyl carbonate (1:1, v/v ratio) (Merck) was used as the electrolyte. The galvanostatic cycling and cyclic voltammetry (CV) tests were performed between 2.5 and 4.6 V at room temperature using computer controlled Arbin battery (Model BT2000, USA) and VMP3 (Bio-Logic SA, France) testers. AC impedance spectra were recorded using VMP3 tester coupled with frequency response analyzer in frequency range of 10 mHz to 500 kHz.

(ii) $Li_4Ti_5O_{12}$ synthesis and material characterization

For synthesis of LTO, 0.01M of cetyl trimethylammonium bromide (CTAB) surfactant was dissolved in ethanol-water solution with a volume ratio of 3:1. The starting materials, lithium acetate hydrate ($LiOOCCH_3.H_2O$) and titanium isopropoxide ($C_{12}H_{28}O_4Ti$) in a stoichiometric molar ratio were added into the prepared CTAB-ethanol solution. The solution was stirred for 24-60 hour (h) and dried using rotor evaporator at temperature 70-80 °C. After drying, the obtained powder was sintered in tube furnace under Air at 700-800 °C for 6-12 h.

The phase of LTO was characterized by X-ray diffraction (XRD) 6000 SHIMADZU, Japan with Cu-K_α radiation (λ = 1.54056 Å). The morphology and microstructure of obtained powder were investigated by HITACHI S4300 field emission scanning electron microscopy (FESEM) at 15 kV and

transmission electron microscopy (TEM) at 200 kV (JEOL-2010F). The LTO electrodes were prepared by mixing active material, super P/Denka black and polyvinylidene difluoride (PVDF) (Kynar 2801) at a weight ratio of 75:15:10 (90:5:5 ratio for 18650 cells) in N-methyl-2-pyrrolidone (NMP) solvent. Then, electrodes were prepared using an etched copper/aluminium foil as current collector via doctor-blade technique. Electrochemical performances of electrodes were investigated using CR2016 coin-type cells. The coin cells were assembled in argon-filled glove box (MBraun, Germany). Whatman binder-free glass microfiber filter (type GF/F) was used as the separator, lithium metal foil was used as the anode, and 1-M lithium hexafluorophosphate ($LiPF_6$) in ethylene carbonate/diethyl carbonate (1:1, v/v ratio) (Merck) was used as the electrolyte. The galvanostatic cycling and cyclic voltammetry (CV) tests were performed between 1-2.5 V at room temperature using computer controlled Arbin battery (Model BT2000, USA) and VMP3 (Bio-Logic SA, France) testers.

(iii) Commercial type 18650 cell fabrication

A pilot line set up using the **funding from NUS** was used to fabricate the commercial type 18650 cells. **Figure 4** presents some of the equipment located at the battery pilot line, these equipment were purchased from Eager Corporation, Japan.

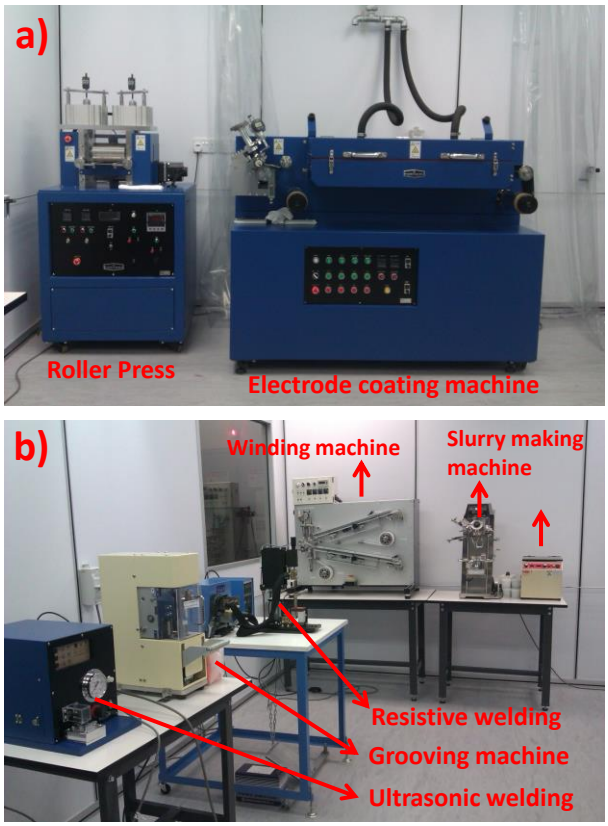

Figure 4 (a) Coating machine and roller press, (b) Ultrasonic welding, grooving, resistive welding, winding machines and slurry making machine.

The LVP or NMC cathode and LTO anode electrodes for 18650 cells were prepared by mixing active material, Denka black and polyvinylidene difluoride (PVDF) (Kynar 2801) at a weight ratio of 90:5:5 (LTO and NMC) and 80:10:10 (LVP) respectively in N-methyl-2-pyrrolidone (NMP) solvent. Then, electrodes were prepared using an etched copper/aluminium foil with the thickness of ~10-15µm as current collector via big coating machine (pilot line-**Figure 4a**). The electrode was pressed around 10-18 kN to ensure intimate contact between the particles and current collector using roller press

(**Figure 4b**). The pressed electrode was slited to required dimension. Electrodes were welded with Al/Ni tag using ultrasonic welder (**Figure 4b**). NMC cathode and LTO anode jelly was fabricated using winding machine using celgard as separator. Then, the jelly was fixed into Al can with the insulator. Ni tag was welded with the bottom of the can using resistive welding while the Al tag was welded to the cap ultrasonically. The electrolyte was filled into the cell using electrolyte filling machine (**Figure 5**). A complete flow chart for commercial cell fabrication is show in the **Figure 5**. Electrochemical performances of electrodes were investigated using 18650 cells. The 18650 cells were assembled in argon-filled glove box (MBraun, Germany). Celgard polymer was used as the separator and 1-M lithium hexafluorophosphate ($LiPF_6$) in ethylene carbonate/diethyl carbonate (1:1, v/v ratio) (Merck) was used as the electrolyte. The galvanostatic cycling tests were performed between 1.55-3 V at room temperature using computer controlled high current (10 A) Arbin battery (Model BT2000, USA).

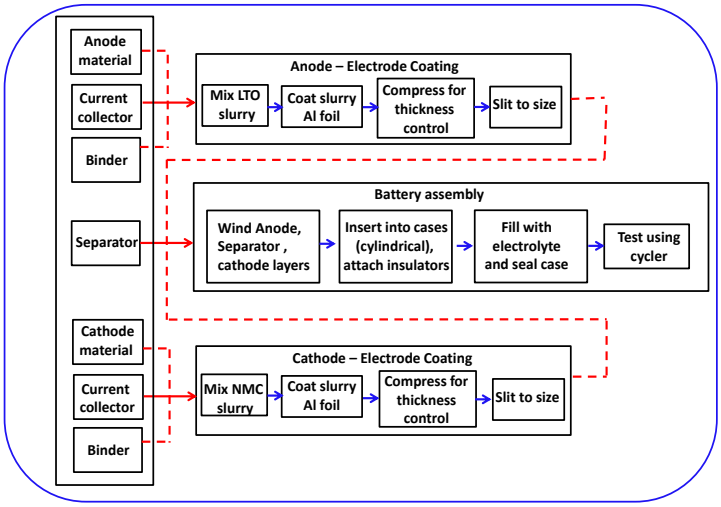

Figure 5 Flow chart for commercial battery fabrication using battery pilot line

C. Results and Discussion

(i) Fundamental contribution

Morphology and Structure of $Li_3V_2(PO_4)_3$

It is clear from the Rietveld refinement of measured XRD pattern (**Figure 6**) that the monoclinic phase LVP is formed. The fit between the calculated and measured XRD patterns was excellent with weighted factor R_{wp} of 4.00 %. The considerably small R_{wp} factor implies that single phase monoclinic LVP can be obtained by our synthesis method and no other impurities phases such as Li_3PO_4 and V_2O_3 are observed. The unit cell parameters for the obtained material were a = 8.6095 Å, b = 8.6041 Å, c = 12.0560 Å and β = 90.490° and its cell volume was estimated to be 893.044 $Å^3$. All the diffraction peaks can be well indexed to monoclinic LVP crystal structure (ICDD PDF: 01-074-3236, 2011 International Centre for Data Diffraction) with space group $P2_1/n$.

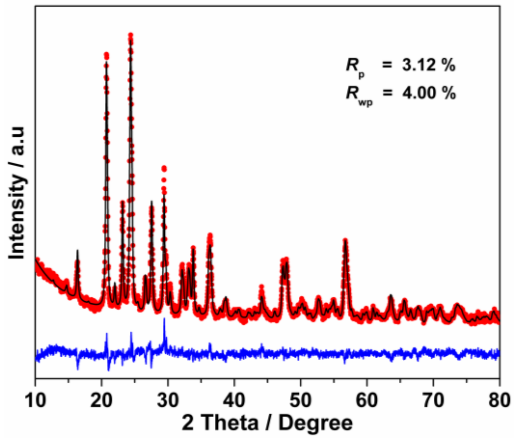

Figure 6 XRD Rietveld refinement of LVP/C. Measured profile: red points; calculated: black line, difference: blue line

FESEM shows that the LVP/C powder composed of aggregated particles with average secondary particle size in the range 200-300 nm (**Figure 7 (a-b)**). Upon observation under high magnification, the particles found to be constructed from interconnected porous nano-particles with average grain size around 20-50 nm. The most severe limitation of LVP/C is its considerably low electronic conductivity. In order to achieve superior electrochemical performance at high rate it is mandatory to have good conductive wiring among the surface of LVP/C particles. This electronic wiring must be permeable to lithium ions and efficient in transferring the electrons into/from the LVP surface to the corresponding current collector.

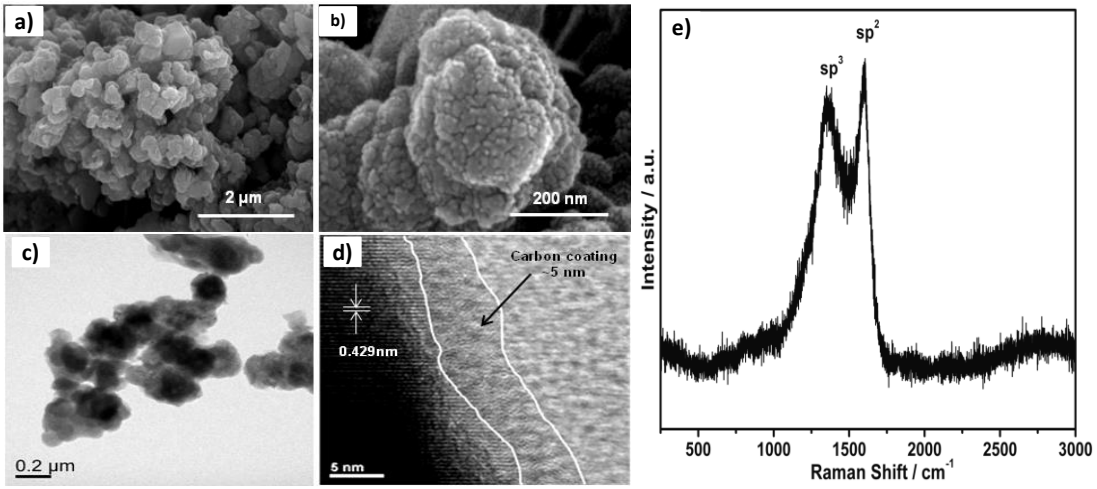

Figures 7 (a-b) FESEM images of LVP/C at different magnifications, (c) TEM, (d) HRTEM images and (e) Raman spectrum of LVP/C

High resolution transmission electron microscopy (HRTEM) image showed carbon coating on the surface of LVP particles, the thickness was estimated around 5 nm (**Figure 7c, d**). The presence of *in-situ* carbon not only suppresses the growth of LVP particles during calcination, it also provides good electronic contact between LVP particles due to its uniform distribution throughout the sample. Clear lattice fringes observed from the HRTEM image (**Figure 7d**) indicate high crystalline nature of obtained LVP/C. The measured width of neighbouring lattice fringes was approximately 0.429 nm which corresponded well to the (002) plane of LVP (**Figure 7d**).

The nature of carbon coating for the synthesized LVP/C was characterized by Raman spectroscopy. As

shown in **Figure 7e**, the Raman spectrum showed two intense broad bands at 1362 and 1599 cm^{-1}, which can be attributed to the D (disordered) and G (graphene) bands of carbon coated on the surface of LVP particles. The content of sp^3 and sp^2 carbon in the LVP/C can be determined by the relative intensity ratio of D and G bands. Generally, the increase of sp^2 type carbon or the decrease of D/G ratio can improve the electronic conductivity resulting in excellent rate capability and discharge capacity. From the analysis, the I_D/I_G ratio of synthesized LVP/C was around 0.91. This indicates that the synthesized LVP/C compound contains slightly higher amount of graphene (sp^2) type conductive carbon than the disordered carbon (sp^3) which is favourable for improving the rate performance.

Electrochemical characteristics of $Li_3V_2(PO_4)_3$

Figure 8a depicts the electrochemical performance of tailored LVP/C against lithium metal with different voltage window, delivering differential capacity with various voltage profiles (**Figure 8b**). Until upper cut-off voltage of 4.3 and 4.4 V, vs. Li/Li^+ respectively which corresponds to redox couple of V^{3+}/V^{4+}, the battery delivered a discharge capacity of ~133 mAh g^{-1} which corresponds to extraction/insertion of two moles of lithium with flat voltage steps during charge and discharge. On the other hand, beyond 4.4 V (4.45, 4.5, 4.55, 4.6 V) the discharge process during lithium insertion showed an initial S-shaped curve of single-phase region followed by two phase transition behaviour (**Figure 8a**).

The electrochemical voltage composition profiles with two and three moles of lithium extraction/insertion is shown in **Figure 8(c-d)**, resulting in differential capacity and voltage with respect to the site potential of the lithium and interaction with $V^{3+}/V^{4+}/V^{5+}$ redox couples in the lattice structure.[32-36] Figure 8a shows the charge/discharge voltage profiles of LVP/C at 0.1C rate in the voltage window of 2.5-4.3V. Under this restricted voltage window, two lithium per formula unit are removed in three voltage steps. These two lithium ions are extracted at the potential of 3.59, 3.67 and 4.07 V vs. Li/Li^+ respectively which corresponds to redox couple of V^{3+}/V^{4+}, delivered a discharge capacity of 133 mAh g^{-1}. The very low degree of overpotential in the redox reaction shows that the ionic and electronic transport is rapid in removal of first two lithium ions from the lattice. Since, the third lithium is extracted at the potential of 4.54 V as shown in **Figure 8d**, an extended voltage window (2.5-4.6 V) allows the extraction of third lithium ion from the framework.

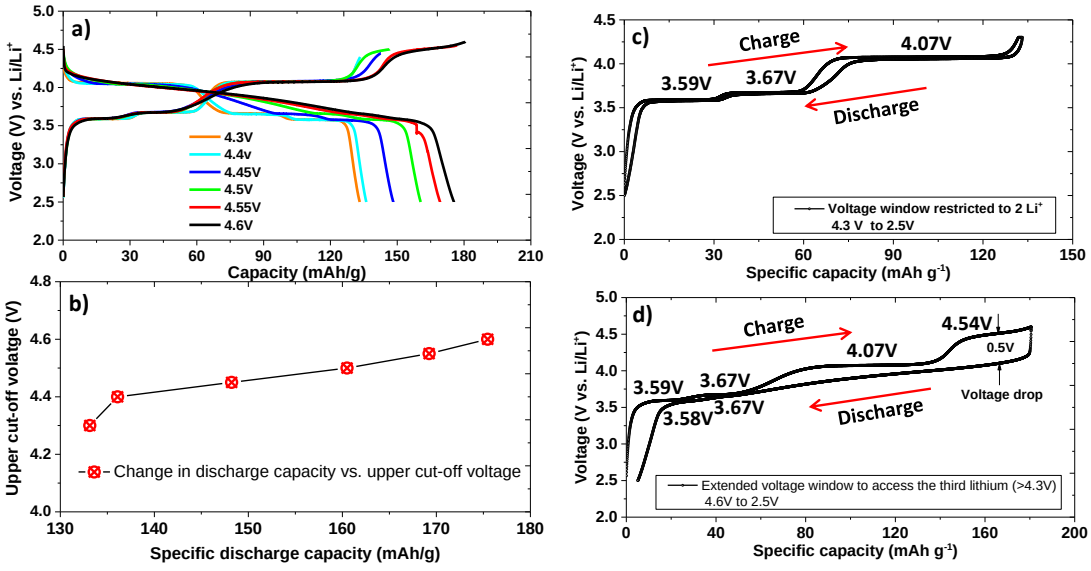

Figure 8 (a) Electrochemical voltage profiles of LVP with different voltage, (b) Specific discharge capacity with various upper cut-off voltage. Electrochemical voltage composition profiles of $Li_xV_2(PO_4)_3$, x=3, 2.5, 2, 1 and 0 with different moles of extraction/insertion, (c) two moles of lithium and (d) three moles of lithium.

Under this wider voltage window, all three lithium ions per formula unit are extracted in four voltage plateaus at around 3.59, 3.67, 4.07 and 4.54 V during charge, which are associated with the two-phase transition process of $Li_xV_2(PO_4)_3$ (x = 3.0, 2.5, 2.0, 1.0, and 0). The removal of the all three lithium ions is associated with the redox reaction of $V^{3+}/V^{4+}/V^{5+}$. During charging, the first lithium ion was extracted in two steps at the voltage plateaus of 3.59 and 3.67 V due to the existence of an ordered phase of $Li_{2.5}V_2(PO_4)_3$.[14] This was followed by the removal of second lithium ion at a single voltage plateau of 4.07 V to form $LiV_2(PO_4)_3$. All of these three successive voltage plateaus signify the two-phase character of electrochemical reaction in the associated composition range and they correspond to V^{3+}/V^{4+} redox couple (**Figure 8**). Further, the removal of third lithium ion associated with the redox couple of V^{4+}/V^{5+} occurs at 4.54 V vs. Li/Li^+. Most significant is that the higher overpotential at V^{4+}/V^{5+} redox reaction (~0.5 V) than the V^{3+}/V^{4+} redox reaction, suggests that the lithium ion kinetics is initially faster and slow down only when x=2 in $Li_{3-x}V_2(PO_4)_3$.[37,38] On the other hand, the discharge process showed an initial S-shaped curve of single-phase region followed by two phase transition behaviour at voltage plateaus around 3.67 and 3.59 V (though not seen obviously). The initial discharge capacity of the prepared material can reach 178 mAh g^{-1} with coulombic efficiency of 91.3%.

The phase transition is due to the site potential of the lithium, interaction with V^{n+} and mixed valence state of V^{4+}/V^{5+} upon insertion of third lithium in to the framework, not due to changes in the structure (**Figure 9**).[36] The observed voltage profiles during charge and discharge are the characteristic of the lithium extraction and insertion reactions of LVP.

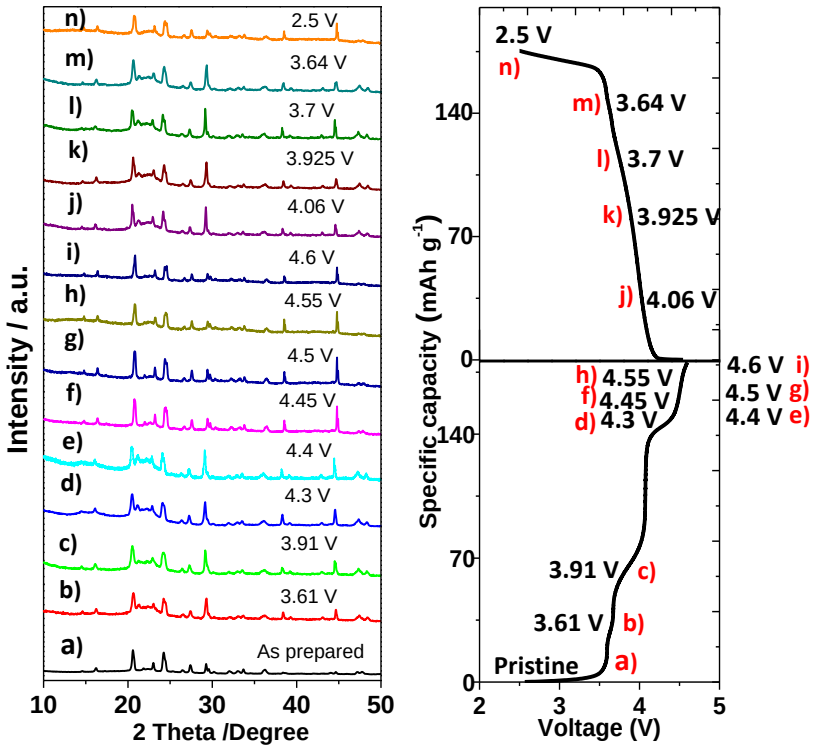

Figure 9 XRD patterns at, (a) x=3, starting phase; (b) extraction at 3.61 V, x=2.5; (c) extraction at 3.91 V, x=2; (d) extraction at 4.3 V, x=1; (e) extraction at 4.4V, x=1, (f) extraction at 4.45V, x<1; (g) extraction at 4.5 V, x<1; (h) extraction at 4.55 V, x<1; (i) extraction at 4.6 V-end of charge, x<1; (j) insertion at 4.06 V, x<1; (k) insertion at 3.925 V, x=1; (l) insertion at 3.7 V, x=2; (m) insertion at 3.64 V, x>2; (j) insertion at 2.5 V, x=3 and corresponding electrochemical profiles with extraction and insertion points.

Further, reversible extraction/insertion electrochemical process is confirmed by XRD pattern at

various stages of charging and discharging cycle. XRD patterns of x=3 are identical at end of the discharge and XRD of pristine material (**Figure 9n and 9a**). Further XRD patterns of x=2 are comparable during extraction and insertion (**Figure 9d, 9e and 9l**). Though charging process follows two-phase transition upon extraction of x>2 lithium, there is a difference in the diffraction pattern beyond 2 lithium (>4.4V) (**Figure 9f-9i**). The XRD patterns are identical at 4.45, 4.5, 4.55 and 4.6 V. Further, XRD patterns of x=1 are different during extraction/insertion of lithium (**Figure 9c and 9k**).

ESR measurement on $Li_3V_2(PO_4)_3$

ESR measurements were carried out, in order to investigate the changes in the local coordination of vanadium ions and to check their valence states during the electrochemical cycling for the best performing LVP/C (vs. Li/Li^+) cell, the cells were dismantled after fully charging and discharging to 4.6 V and 2.5V respectively. V^{3+} ion has d-electronic configuration $3d^2$ and ground state ^3F with spin $S = 1$. For such ion with an even number of electrons in the respective electronic shells singlet ground-state levels may result such that no ESR is observable. Indeed, we do not observe the ESR signal in as-prepared LVP/C samples which would be expected for vanadium ions in [3+] valence state. At the same time, by perfoming the ESR at low temperatures, we able to resolve a weak resonance signal in the ESR spectra of as-prepared compound which will be discussed later.

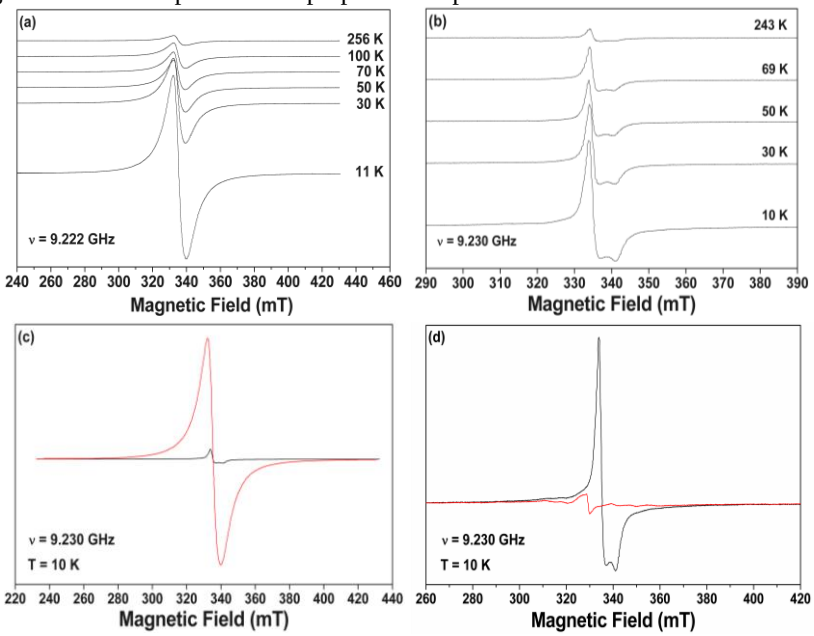

Figure 10 ESR spectra of (a) delithiated LVP/C and (b) as-prepared LVP/C; ESR spectra of as-prepared (black line) and (c) fully delithiated (red line) as well as (d) relithiated (red line) LVP/C normalized to the mass

ESR spectra of delithiated LVP/C are shown in **Figure 10a**. Approximation of these spectra yielded the best fit of experimental data for the powder spectrum, corresponding to the paramagnetic centers with effective spin $S = 1/2$ and anisotropic g-factor $g_\perp = 1.974$, $g_\parallel = 1.936$. Obtained anisotropic g-factor was close to the g-factor of V^{4+} ions in tetragonally distorted VO_6 octahedra [39]. This was consistent with the electrochemical performance results, according to which vanadium changed its valency state from [3+] to [4+/5+] during charging. It should be noted that V^{5+} ion has no electrons in 3d electron shell and therefore this ion is ESR silent. Since vanadium has a nuclear spin $I = 7/2$, ESR spectra of V^{4+} ions are expected to contain 8 lines of hyperfine structure due to the interaction of the electron spin ($S = 1/2$) with the nuclear spin of ^{51}V. The absence of hyperfine structure of V^{4+} ion in the ESR spectra of delithiated LVP/C can be associated with the presence of exchange interactions between vanadium ions.[40] Exchange interactions between magnetic ions in such magnetically concentrated compounds lead to the merging of hyperfine-structure lines into a single absorption line located at the center of gravity of the hyperfine lines.

ESR spectra of as-prepared LVP/C are shown in **Figure 10b**. Approximation of these spectra yielded the best fit of experimental data for the powder spectrum, corresponding to paramagnetic centers with effective spin $S = 1/2$ and anisotropic g-factor $g_{\perp} = 1.972$, $g_{\parallel} = 1.928$. It can be seen that the paramagnetic centers determining the ESR spectra of the as-prepared and the delithiated phases of LVP/C had similar resonance parameters. This suggests that ESR spectra of as-prepared compound correspond to V^{4+} ions. The presence of V^{4+} ions in the initial samples of LVP/C can be associated with small lithium non-stoichiometry. It is known that the integral intensity of absorption line is proportional to the concentration of paramagnetic centers. This fact allows us to determine the relative concentration of V^{4+} ions in the as-prepared and delithiated phases of LVP/C. As can be seen from **Figure 10c**, the intensity of ESR spectrum of as-prepared LVP/C was much smaller than that of the delithiated one. The estimation of V^{4+} ions' concentration in the as-prepared samples of LVP/C gave the value of 1.5 %.

It should be noted that ESR signal discussed above was not observed in the ESR spectrum of relithiated LVP/C which had the same composition as as-prepared LVP/C (**Figure 10d**). This indicates that vanadium ions giving rise to the ESR signal in the as-prepared samples change their valence state during the cycling of LVP/C cell. According to electrochemical performance results, the most probable change of valence state of these ions after one charge/discharge cycle is their reduction to the V^{3+} ions. Since V^{3+} ions are ESR silent in our experiments, the proposed changes in the valence state of vanadium ions are consistent with ESR data. The reduction of all vanadium ions to the valence state [3+] after the first charge/discharge cycle corresponds to reversible intercalation of all lithium ions to the LVP/C. Thereby, the host structure of LVP/C samples allows using its maximum capacity during the first charge/discharge cycle.

High rate performance of $Li_3V_2(PO_4)_3$

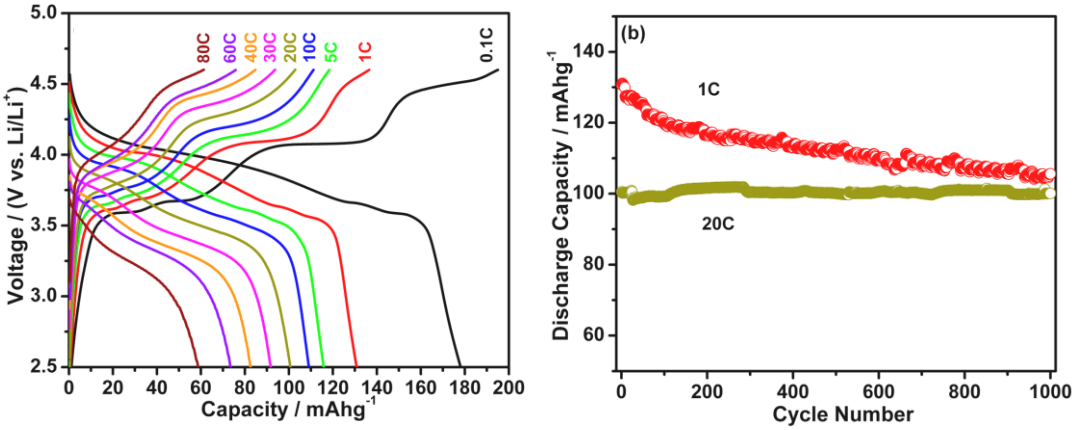

Figure 11 (a) Electrochemical charge/discharge curves of LVP/C calcined at 800 °C for 6 h at different C rates in voltage window 2.5-4.6 V and (b) long-term cyclability at 1C and 20C up to 1000 cycles in voltage window 2.5-4.6 V, testing was performed at room temperature.

Figure 11a shows the cycle life performance of LVP/C at different C rates in the voltage window of 2.5-4.6 V. The initial discharge capacity was 178 $mAhg^{-1}$ and it decreased to 157 $mAhg^{-1}$ after 25 cycles at 0.1C. Fading was also found in previous studies.[41,42] The capacity fading could be due to the dissolution of vanadium in electrolyte as reported in literatures.[10,43,44] Nevertheless, LVP/C still exhibited excellent cycle performance at high rates. At high rate, the exposure time of vanadium to electrolyte is lesser than the low rate. Therefore, the dissolution of vanadium in the electrolyte can be minimized and this could possibly lead to its stable cycle performance at high rate. At 1C rate, the initial discharge capacity was 131 mAh g^{-1} with a coulombic efficiency of 92.8 %. After 25 cycles, it can sustain discharge capacity of 128 mAh g^{-1} with coulombic efficiency of 96.5 %. With further storage performance up to 1000 cycles (**Figure 11b**), the discharge capacity decreased to around 105

$mAhg^{-1}$ (80.2 % of its initial capacity). In the case of higher C rate, for example at 20C, LVP/C can provide initial discharge capacity of 100 $mAhg^{-1}$ and it can retain its discharge capacity of around 100 $mAhg^{-1}$ without significant fading at 1000 cycles (**Figure 11b**), which can reiterate the material's stability at high rate. Such stable high rate cycle performance and the capability of nanostructured mesoporous LVP/C to deliver discharge capacity up to 80C indeed would be attractive for future defense applications.

(ii) Development of Li-ion battery technology:

Production and scale-up of LTO anode

LTO anode material was produced using simple, one pot soft temple synthesis process. **Figure 12** shows schematic illustration of LTO production and more detail about the synthesis process mentioned in the experimental section.

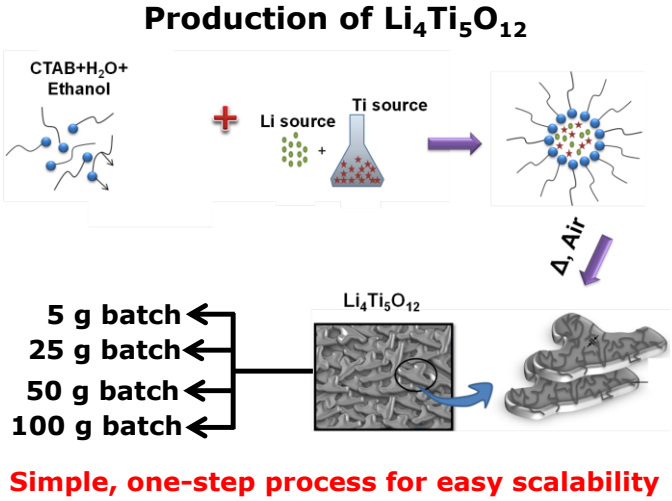

Figure 12 Schematic illustration of LTO synthesis

Electrochemical performances of 5g and 25g batch of LTO were shown in the **Figure 13**. 5g batch LTO sample has delivered a charge capacity of 157 mAh g^{-1} at 0.2C with the coulombic efficiency of 96.31%. LTO material synthesized by soft template method exhibits pseudo-rectangular morphology; the particles size in range of 300-500 nm with the surface area of 6 m^2 g^{-1}. LTO sample prepared by 25g batch synthesis, delivered a charge capacity of 153 mAh g^{-1} at 0.2C with the coulombic efficiency of 96.83%.

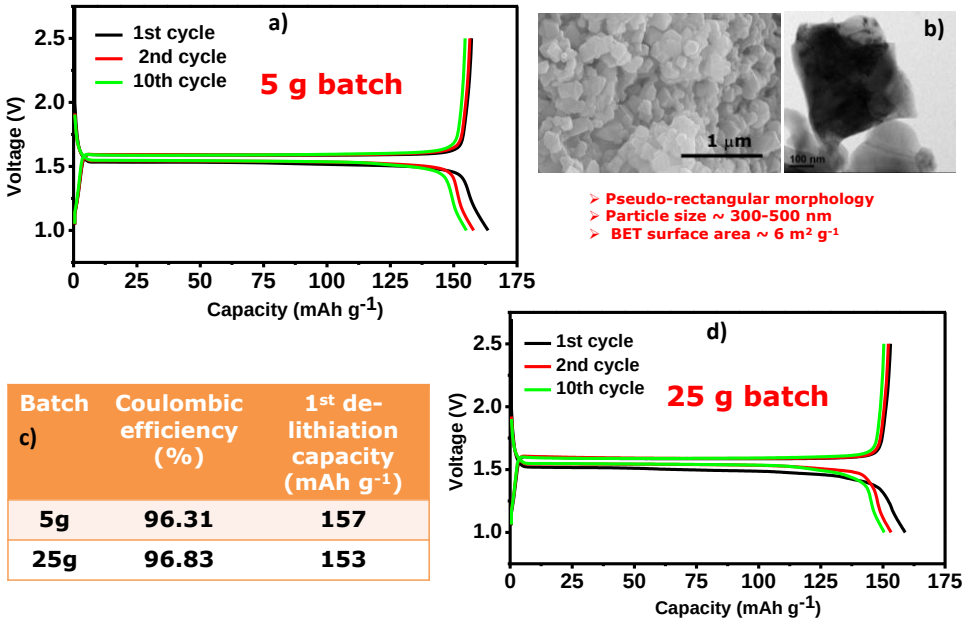

Batch c)	Coulombic efficiency (%)	1st de-lithiation capacity (mAh g^{-1})
5g	96.31	157
25g	96.83	153

Figure 13 (a) Charge/discharge profiles of LTO of 5 g batch at 0.2C rate; (b) morphology of LTO; (c) discharge capacity and coulombic efficiency of 5 and 25 g batch at 0.2C rate and (d) Charge/discharge profiles of LTO of 25 g batch at 0.2C rate.

We have also tested rate performance in the coin cells vs. Li/Li$^+$ at different C rates of 25g batch material. This material exhibited charge capacities of 152, 123, 100, 69 and 52 mAh g^{-1} at 1C, 10C, 20C, 40C and 60C respectively (**Figure 14a**). This material also exhibited capacity retention of 93% after 300 cycles and coulombic efficiency over 100% (**Figure 14b**). Further, we had fabricated coin cells with the material from 50 and 100g batch synthesis, they showed charge capacities of ~163 and ~162 mAh g^{-1} respectively, at 0.1C rate (**Figure 15**). This shows the repeatability of our simple, one step soft template synthesis.

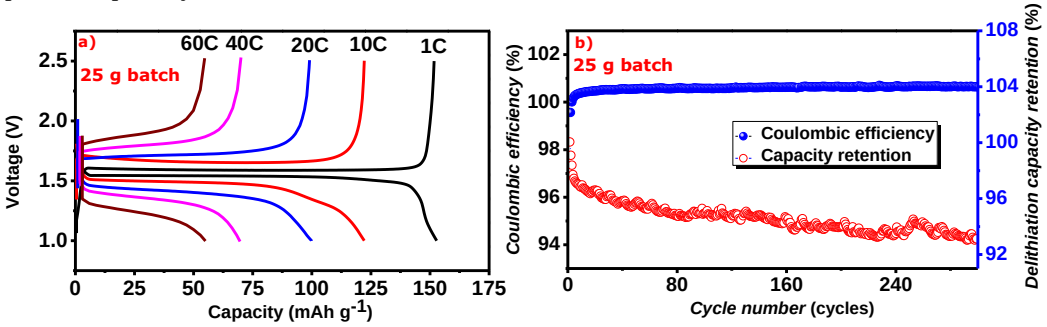

Figure 14 (a) Charge and discharge capacity of LTO of 25 g batch at different C rates and (b) discharge capacity retention and coulombic efficiency of 25 g batch up to 300 cycles at 1C rate.

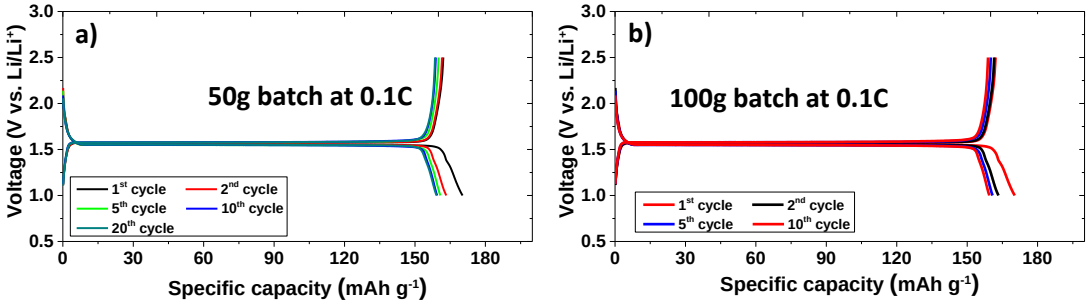

Figure 15(a) Charge/discharge capacity of LTO of 50g batch at 0.1C rate up to 20cycles and (b) Charge/discharge capacity of LTO of 50g batch at 0.1C rate up to 10cycles.

(iii) Device fabrication: 18650 cell

Electrochemical characterization of LVP vs. LTO

Initially, the electrochemical performance of this novel combination of LVP vs. LTO was tested using coin cells over the voltage window of 1.5-3V, where we can extract/ insert close to three moles of lithium. The electrochemical performance of this chemistry is shown in the **Figure 16**. With this voltage window (1.5-3V), the full cell exhibited first cycle discharge capacity of 184 mAh g^{-1} at 0.5C rate with S-shaped curve in the discharge profiles which is the signature of extraction/insertion of third lithium as seen in the half-cell performance profiles (**Figure 16a**). After 10 cycles, it had shown discharge capacity of 149 mAh g^{-1} at 0.5C rate. This suggests that the capacity retention is not good. Further, this material had delivered discharge capacities of 139 and 85 mAh g^{-1} at 1C and 5C respectively with the voltage window of 1.5-3 V at room temperature (**Figure 16b-16c**).

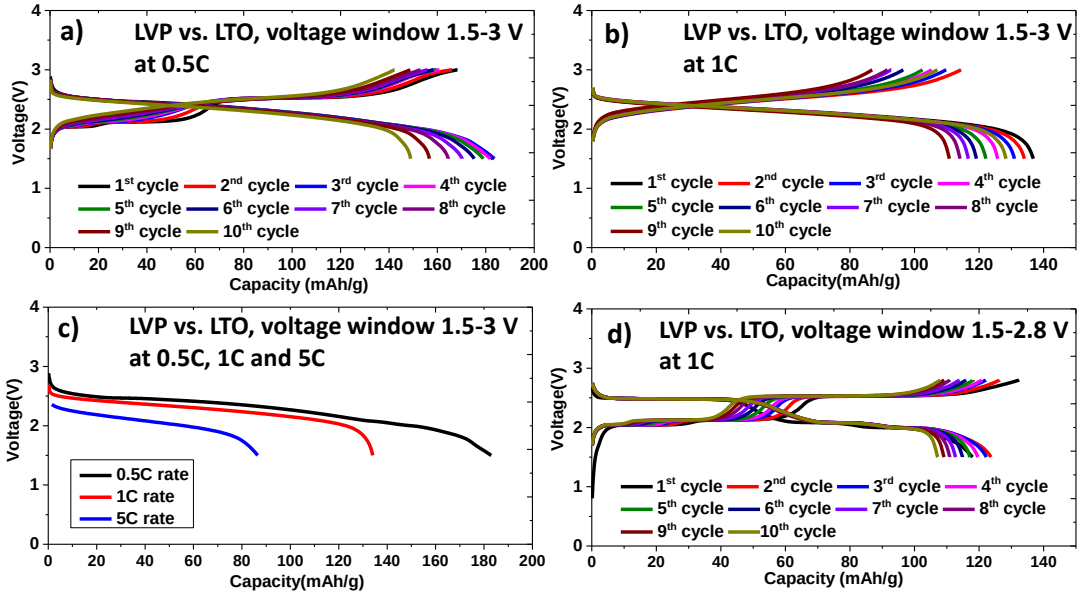

Figure 16 Electrochemical performance of full-cell combining LVP vs. LTO at room temperature; (a) charge/discharge profiles of LVP vs. LTO at 0.5C with voltage window of 1.5-3 V, (b) charge/discharge profiles of LVP vs. LTO at 1C with voltage window of 1.5-3 V, (c) discharge capacity of LVP vs. LTO at different C rates with voltage window of 1.5-3 V and (d) charge/discharge profiles of LVP vs. LTO at 1C with voltage window of 1.5-2.8 V.

Figure 16d showed lithium storage performance of LVP vs. LTO with the restricted voltage of 1.5-2.8 V where only two moles of lithium can be extracted/inserted into/from the structure. This

electrochemical cell only exhibited discharge capacity of 124 mAh g^{-1} at 1C rate (**Figure 16b**) with three distinct voltage plateaus in both charge and discharge curves and slightly low discharge capacity compared to wider voltage window (1.5-3 V), depicted 139 mAh g^{-1} at 1C rate with the S-shaped curve (**Figure 16d**).

Figure 17 LVP electrodes with high loading, coated using coating machine in the pilot line; material come off after roller pressing.

After performance evaluation using coin cells, we had prepared LVP electrodes on the aluminium substrate using coating machine in the pilot line. The electrode was then pressed using roller press to create intimate contact between the particles and with the aluminium substrates. However we found that the adhesion between the electrode material and the aluminium substrate was poor owing to fluffy nature of the active material and high in-situ carbon content (**Figure 17**). Currently we are aiming to improve the adhesion problem. In view of this failure to prepare good electrodes using LVP for 18650 cells, we had extended our work in combining commercial NMC cathode material with our potential in-house LTO anode material to develop 18650 cells.

Electrochemical characterization of NMC/LTO 18650 cell

Figure 18 shows the NMC cathode electrode coated on aluminum foil. This electrode has been cut to length of 50 cm, slit to width of 50 mm (**Figure 18a**). The Al tag was welded ultrasonically to one end of electrode (**Figure 18b**) and dried at 100 °C overnight using vacuum oven.

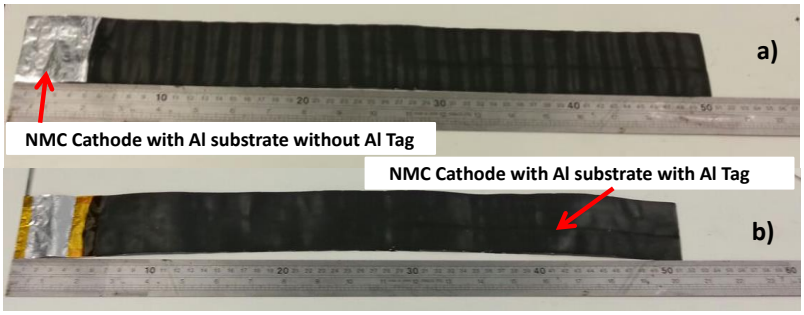

Figure 18 NMC cathode coated on Al foil; (a) without Al Tag and (b) with Al Tag welded ultrasonically

Figure 19 shows the LTO anode electrode coated on copper foil. This electrode has been cut to length of 50 cm, slit to width of 52 mm (**Figure 19a**). Then Ni tag was welded ultrasonically in one end of electrode (**Figure 19b**) and dried at 100 °C overnight using vacuum oven.

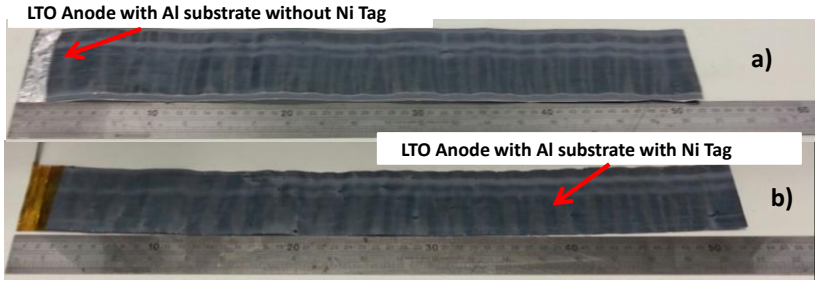

Figure 19 NUS LTO anode coated on Al foil; (a) without Ni Tag and (b) with Ni Tag welded ultrasonically

The electrodes were pressed at 10-14 kN using roller press to ensure intimate contact between the particles and current collectors. Electrodes were welded with Al/Ni tag using ultrasonic welder. NMC/LTO jelly was fabricated by winding machine using celgard as separator. Ni tag was welded with the bottom of the can using resistive welding while the Al tag was welded to the cap ultrasonically. After attaching the cap, the cells were moved into an Argon glove box for electrolyte filling and crimping. Upon assembly, OCV of the cell was measured. **Figure 20** shows NUS-18650 cell fabricated using NMC cathode and LTO anode.

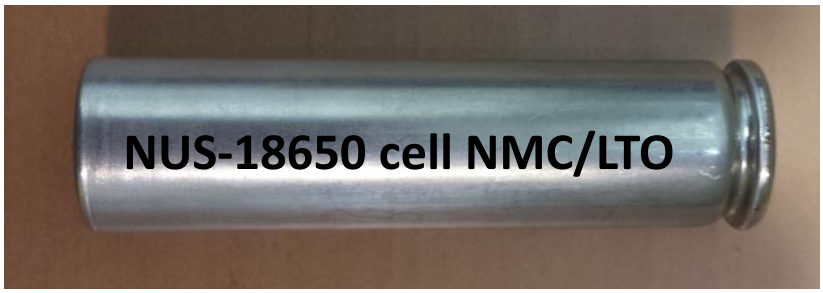

Figure 20 NUS-built 18650 NMC/LTO cell

Electrochemical tests were performed on novel 18650 NMC/LTO batteries by means of Constant Current–Constant Voltage (CC–CV) cycling mode (CC–CV mode only at the charge state, not at the discharge state) with a voltage window of 1.55V-3V at room temperature using an Arbin battery tester (Model, BT2000, USA) (**Figure 21, 22**).

Batch A:

The lithium storage and rate performances of NMC/LTO 18650 battery cell were tested. Batch A 18650 cells exhibited discharge capacity of 850 mAh . **Figure 21** shows the rate performance of this 18650 cell and the battery was tested at various C rates viz. at 0.2C, 0.5C and 1C rates. At 0.2C rate, this battery has exhibited lithium storage capacity of ~900 mAh (0.90Ah) (**Figure 21b**). The performance was tested for about 10 cycles, where the capacity stabilized at 850 mAh. As seen from the graph the cycling showed good capacity retention at the discharge with the average operating voltage of 2.3 V.

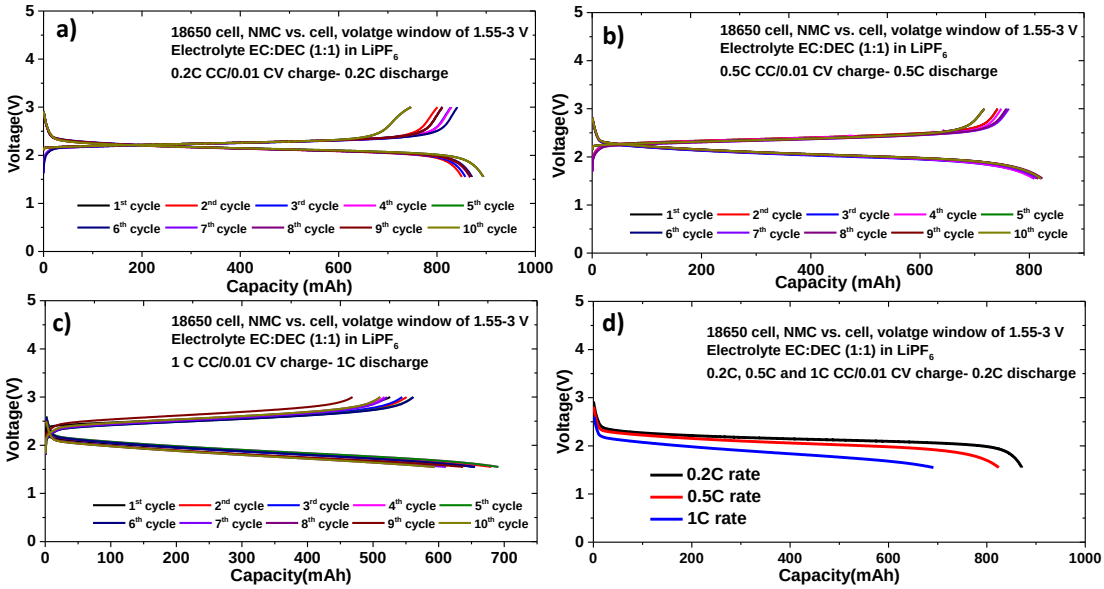

Figure 21 (a) NMC vs. LTO 18650 cell developed in our in laboratory with the energy density of 54 Wh/kg; Electrochemical performance of novel 18650 NMC vs. cell at various current rates up to 10 cycles; (b) 0.2C, (c) 0.5C, (d) 1C and (e) discharge profiles at different C rates at room temperature.

At 0.5C rate the battery showed a capacity of ~805mAh (**Figure 21c**). The cycling at 0.5 C rates also showed good capacity retention for about 10 cycles, but as seen from the graph the polarization increased at this C rate. Nevertheless the columbic efficiency and the capacity retention of the battery are maintained as in the case of 0.2C rate. Galvanostatic cycling was also done at 1C rate (i.e. 1 hr of charging/discharging). The cycling at 1C rate has given a capacity of about 700 mAh (**Figure 21d**). The voltage polarization had increased at this C rate compared to other slow C rates (**Figure 21b-21e**).

Batch B:

In order to increase the storage capacity of NMC/LTO 18650 cell, we have fabricated Batch B high energy density NMC/LTO battery. As shown in **Figure 22**, the storage capacity of Batch B NMC/LTO cell increased to 1054 mAh, the energy density of which is estimated to be 63 Wh/kg (battery total weightis 38.4 g). As seen from the graph the cycling showed good capacity retention at the discharge with the average operating voltage of 2.3 V. The lithium storage performance of 18650 batch B was not impressive at high current rates compared to batch A. To improve the energy density, especially power density and to reduce voltage polarization of 18650 NMC vs. LTO cell chemistry, inde ed active material (NMC and LTO), carbon and binder content needs to be optimized. Work i s in progress to improve the rate performance of batch B.

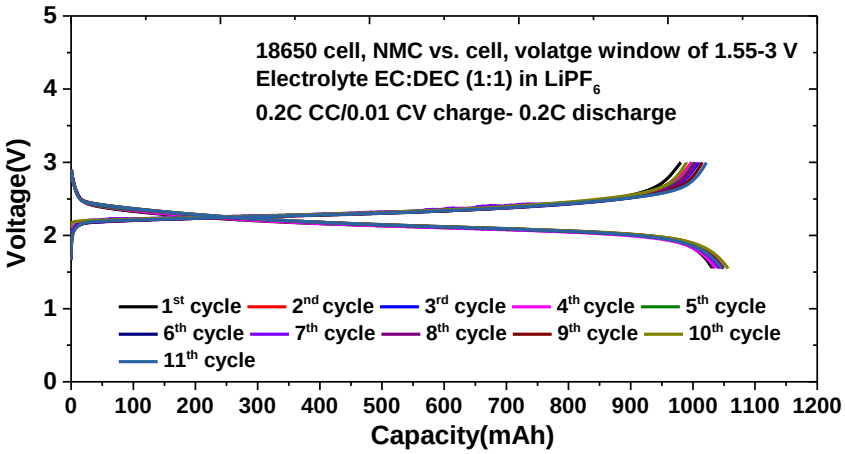

Figure 22 Electrochemical performance of novel 18650 NMC vs. cell developed in our in laboratory with the energy density of 63 Wh/kg up to 11 cycles.

Key highlights

- LVP cathode material was developed and scaled up over 50g in one pot successfully
- Demonstrated high rate performance and long term cyclability of LVP can be improved by preparing electrode material with a favourable architecture.
- Addressed the causes for the observed high rate performance in LVP.
- Titanium-based anode material LTO was developed and scaled up over 100g in one step for the novel 18650 cells.
- Novel 18650 cell chemistry was fabricated using in-house scaled up LTO with commercial NMC cathode material with the energy density of 63 Wh/kg which has comparable performance to the commercial LTO-based batteries. Further work is in progress to improve energy density and power density using alternative cathode material against LTO along with fabrication conditions.

Future work and suggestion

- To improve the quality of the LVP electrodes, the material has to be prepared with dense particles and minimum *in-situ* carbon.
- To improve the energy density, especially power density and to reduce voltage polarization of novel 18650 NMC vs. LTO cell chemistry, indeed active material (NMC and LTO), carbon and binder content needs to be optimized.
- Indeed electrolyte content/constituent and 18650 cell fabrication has to be improved to achieve good rate performance.

List of Publications and Significant Collaborations that resulted from your AOARD supported project: In standard format showing authors, title, journal, issue, pages, and date, for each category list the following:

a) papers published in peer-reviewed journals: Nil
b) papers published in peer-reviewed conference proceedings: Nil
c) papers published in non-peer-reviewed journals and conference proceedings:
d) conference presentations without papers: 5 (see page no. 21),
e) manuscripts submitted but not yet published, 1 (see page no. 21)
f) provide a list any interactions with industry or with Air Force Research Laboratory scientists or significant collaborations that resulted from this work.

Attachments: Publications a), b) and c) listed above if possible: N.A.

DD882: As a separate document, please complete and sign the inventions disclosure form: N.A.

Important Note: If the work has been adequately described in refereed publications, submit an abstract as described above and refer the reader to your above List of Publications for details. If a full report needs to be written, then submission of a final report that is very similar to a full length journal article will be sufficient in most cases. This document may be as long or as short as needed to give a fair account of the work performed during the period of performance. There will be variations depending on the scope of the work. As such, there is no length or formatting constraints for the final report. Keep in mind the amount of funding you received relative to the amount of effort you put into the report. For example, do not submit a $300k report for $50k worth of funding; likewise, do not submit a $50k report for $300k worth of funding. Include as many charts and figures as required to explain the work.

References

1 Padhi, A. K., Nanjundaswamy, K. S. & Goodenough, J. B. Phospho-olivines as Positive-electrode Materials for Rechargeable Lithium Batteries. *J. Electrochem. Soc.* **144**, 1188-1194, doi:10.1149/1.1837571 (1997).

2 Muraliganth, T. & Manthiram, A. Understanding the Shifts in the Redox Potentials of Olivine $LiM_{1-y}M_yPO_4$ (M = Fe, Mn, Co, and Mg) Solid Solution Cathodes. *J. Phys. Chem. C* **114**, 15530-15540, doi:10.1021/jp1055107 (2010).

3 Amine, K., Yasuda, H. & Yamachi, M. Olivine $LiCoPO_4$ as 4.8 V Electrode Material for Lithium Batteries. *Electrochemical and Solid-State Letters* **3**, 178-179 (2000).

4 Deniard, P. *et al.* High Potential Positive Materials for Lithium-ion Batteries: Transition Metal Phosphates. *J. Phys. Chem. Solids* **65**, 229-233, doi:10.1016/j.jpcs.2003.10.019 (2004).

5 Yamada, A. & Chung, S.-C. Crystal Chemistry of the Olivine-type $Li(Mn_yFe_{1-y})PO_4$ and $(Mn_yFe_{1-y})PO_4$ as Possible 4 V Cathode Materials for Lithium Batteries. *J. Electrochem. Soc.* **148**, A960-A967 (2001).

6 Delacourt, C., Poizot, P., Morcrette, M., Tarascon, J. M. & Masquelier, C. One-step Low-temperature Route for the Preparation of Electrochemically Active $LiMnPO_4$ Powders. *Chem. Mat.* **16**, 93-99, doi:10.1021/cm030347b (2004).

7 Ramar, V., Saravanan, K., Gajjela, S. R., Hariharan, S. & Balaya, P. The effect of synthesis parameters on the lithium storage performance of LiMnPO4/C. *Electrochimica Acta* **105**, 496-505, doi:http://dx.doi.org/10.1016/j.electacta.2013.05.025 (2013).

8 Ramar, V. & Balaya, P. Enhancing the electrochemical kinetics of high voltage olivine LiMnPO4 by isovalent co-doping. *Phys. Chem. Chem. Phys.* **15**, 17240-17249, doi:10.1039/C3CP52311J (2013).

9 Masquelier, C., Padhi, A. K., Nanjundaswamy, K. S. & Goodenough, J. B. New Cathode Materials for Rechargeable Lithium Batteries: The 3-D Framework Structures $Li_3Fe_2(XO_4)_3$ (X=P, As). *J. Solid State Chem.* **135**, 228-234, doi:10.1006/jssc.1997.7629 (1998).

10 Huang, H., Yin, S. C., Kerr, T., Taylor, N. & Nazar, L. F. Nanostructured Composites: A High Capacity, Fast Rate $Li_3V_2(PO_4)_3$/Carbon Cathode for Rechargeable Lithium Batteries. *Adv. Mater.* **14**, 1525-1528, doi:10.1002/1521-4095(20021104)14:21<1525::aid-adma1525>3.0.co;2-3 (2002).

11 Rui, X. H., Li, C. & Chen, C. H. Synthesis and Characterization of Carbon-coated $Li_3V_2(PO_4)_3$ Cathode Materials with Different Carbon Sources. *Electrochim. Acta* **54**, 3374-3380, doi:10.1016/j.electacta.2009.01.011 (2009).

12 Pan, A. Q. P. A. Q. *et al.* High-rate cathodes based on Li(3)V(2)(PO(4))(3) nanobelts prepared via surfactant-assisted fabrication. *Journal of Power Sources* **196**, 3646-3649, doi:10.1016/j.jpowsour.2010.12.067 (2011).

13 Morgan, D. *et al.* Experimental and Computational Study of the Structure and Electrochemical Properties of $Li_xM_2(PO_4)_3$ Compounds with the Monoclinic and Rhombohedral Structure. *Chem. Mat.* **14**, 4684-4693, doi:10.1021/cm020348o (2002).

14 Saidi, M. Y., Barker, J., Huang, H., Swoyer, J. L. & Adamson, G. Performance Characteristics of Lithium Vanadium Phosphate as a Cathode Material for Lithium-ion Batteries. *Journal of Power Sources* **119**, 266-272, doi:10.1016/s0378-7753(03)00245-3 (2003).

15 Yin, S. C., Grondey, H., Strobel, P., Anne, M. & Nazar, L. F. Electrochemical Property: Structure Relationships in Monoclinic $Li_{3-y}V_2(PO_4)_3$. *J. Am. Chem. Soc.* **125**, 10402-10411, doi:10.1021/ja034565h (2003).

16 Islam, M. S., Driscoll, D. J., Fisher, C. A. J. & Slater, P. R. Atomic-scale Investigation of Defects, Dopants, and Lithium Transport in the $LiFePO_4$ Olivine-type Battery Material. *Chem. Mat.* **17**, 5085-5092, doi:10.1021/cm050999v (2005).

17 Amin, R., Balaya, P. & Maier, J. Anisotropy of Electronic and Ionic Transport in $LiFePO_4$ Single Crystals. *Electrochemical and Solid-State Letters* **10**, A13-A16, doi:10.1149/1.2388240 (2007).

18 Prosini, P. P., Lisi, M., Zane, D. & Pasquali, M. Determination of the Chemical Diffusion Coefficient of Lithium in $LiFePO_4$. *Solid State Ion.* **148**, 45-51, doi:10.1016/s0167-2738(02)00134-0 (2002).

19 Barker, J., Saidi, M. Y. & Swoyer, J. L. A Carbothermal Reduction Method for the Preparation of Electroactive Materials for Lithium Ion Applications. *J. Electrochem. Soc.* **150**, A684-A688, doi:10.1149/1.1568936 (2003).

20 Saidi, M. Y., Barker, J., Huang, H., Swoyer, J. L. & Adamson, G. Electrochemical Properties of Lithium Vanadium Phosphate as a Cathode Material for Lithium-ion Batteries. *Electrochem. Solid State Lett.* **5**, A149-A151, doi:10.1149/1.1479295 (2002).

21 Fu, P., Zhao, Y. M., Dong, Y. Z., An, X. N. & Shen, G. P. Synthesis of $Li_3V_2(PO_4)_3$ with High Performance by Optimized Solid-state Synthesis Routine. *Journal of Power Sources* **162**, 651-657, doi:10.1016/j.jpowsour.2006.07.029 (2006).

22 Cahill, L. S., Chapman, R. P., Britten, J. F. & Goward, G. R. Li-7 NMR and two-dimensional exchange study of lithium dynamics in monoclinic Li3V2(PO4)(3). *J. Phys. Chem. B* **110**, 7171-7177, doi:10.1021/jp057015+ (2006).

23 Patoux, S., Wurm, C., Morcrette, M., Rousse, G. & Masquelier, C. A Comparative Structural and Electrochemical Study of Monoclinic $Li_3Fe_2(PO_4)_3$ and $Li_3V_2(PO_4)_3$. *Journal of Power Sources* **119**, 278-284, doi:10.1016/s0378-7753(03)00150-2 (2003).

24 Rui, X. H., Ding, N., Liu, J., Li, C. & Chen, C. H. Analysis of the Chemical Diffusion Coefficient of Lithium Ions in $Li_3V_2(PO_4)_3$ Cathode Material. *Electrochim. Acta* **55**, 2384-2390, doi:10.1016/j.electacta.2009.11.096 (2010).

25 Yin, S. C., Strobel, P. S., Grondey, H. & Nazar, L. F. $Li_{2.5}V_2(PO_4)_3$: A Room-temperature Analogue to the Fast-ion Conducting High-temperature γ-phase of $Li_3V_2(PO_4)_3$. *Chem. Mat.* **16**, 1456-1465, doi:10.1021/cm034802f (2004).

26 Orsini, F. *et al.* In situ SEM study of the interfaces in plastic lithium cells. *Journal of Power Sources* **81-82**, 918-921, doi:Doi: 10.1016/s0378-7753(98)00241-9 (1999).

27 Ohzuku, T., Ueda, A. & Yamamoto, N. Zero-Strain Insertion Material of Li[Li[sub 1/3]Ti[sub 5/3]]O[sub 4] for Rechargeable Lithium Cells. *Journal of the Electrochemical Society* **142**, 1431-1435 (1995).

28 Colbow, K. M., Dahn, J. R. & Haering, R. R. Structure and electrochemistry of the spinel oxides LiTi2O4 and LiTiO4. *Journal of Power Sources* **26**, 397-402 (1989).

29 Peramunage, D. & Abraham, K. M. Preparation of Micron-Sized Li[sub 4]Ti[sub 5]O[sub 12] and Its Electrochemistry in Polyacrylonitrile Electrolyte-Based Lithium Cells. *Journal of the Electrochemical Society* **145**, 2609-2615 (1998).

30 Prosini, P. P., Mancini, R., Petrucci, L., Contini, V. & Villano, P. Li4Ti5O12 as anode in all-solid-state, plastic, lithium-ion batteries for low-power applications. *Solid State Ionics* **144**, 185-192, doi:10.1016/s0167-2738(01)00891-8 (2001).

31 http://www.altairnano.com/products/.

32 Atlung, S., West, K. & Jacobsen, T. Dynamic Aspects of Solid Solution Cathodes for Electrochemical Power Sources. *Journal of The Electrochemical Society* **126**, 1311-1321, doi:10.1149/1.2129269 (1979).

33 West, K., Jacobsen, T., Zachau-Christiansen, B. & Atlung, S. Determination of the differential capacity of intercalation electrode materials by slow potential scans. *Electrochimica Acta* **28**, 97-107, doi:http://dx.doi.org/10.1016/0013-4686(83)85091-9 (1983).

34 Jacobsen, T., West, K. & Atlung, S. Discussion of "Electrochemical Potential Spectroscopy: A New Electrochemical Measurement" [A. H. Thompson (pp. 608–616, Vol. 126, No. 4)]. *Journal of The Electrochemical Society* **126**, 2169-2170, doi:10.1149/1.2128906 (1979).

35 Tillement, O. & Quarton, M. Theoretical Study of Ordering Effects During Electrochemical Insertion. *Journal of The Electrochemical Society* **140**, 1870-1876, doi:10.1149/1.2220731 (1993).

36 Yin, S. C., Grondey, H., Strobel, P., Anne, M. & Nazar, L. F. Electrochemical Property: Structure Relationships in Monoclinic Li3-yV2(PO4)3. *J. Am. Chem. Soc.* **125**, 10402-10411, doi:10.1021/ja034565h (2003).

37 Saïdi, M. Y., Barker, J., Huang, H., Swoyer, J. L. & Adamson, G. Performance characteristics of lithium vanadium phosphate as a cathode material for lithium-ion batteries. *Journal of Power Sources* **119–121**, 266-272, doi:http://dx.doi.org/10.1016/S0378-7753(03)00245-3 (2003).

38 Saïdi, M. Y., Barker, J., Huang, H., Swoyer, J. L. & Adamson, G. Electrochemical Properties of Lithium Vanadium Phosphate as a Cathode Material for Lithium-Ion Batteries. *Electrochemical and Solid-State Letters* **5**, A149-A151, doi:10.1149/1.1479295 (2002).

39 Gallay, R., van der Klink, J. J. & Moser, J. EPR Study of Vanadium (4+) in the Anatase and Rutile Phases of TiO_2. *Phys. Rev. B* **34**, 3060-3068 (1986).

40 Abragam, A. & Bleaney, B. *Electron Paramagnetic Resonance of Transition Ions* (Oxford University Press, 1970).

41 Yu, F., Zhang, J. J., Yang, Y. F. & Song, G. Z. Preparation and Electrochemical Performance of $Li_3V_2(PO_4)_3$/C Cathode Material by Spray-Drying and Carbothermal Method. *J. Solid State Electrochem.* **14**, 883-888, doi:10.1007/s10008-009-0882-6 (2010).

42 Chen, Q. *et al.* Electrochemical Performance of the Carbon Coated $Li_3V_2(PO_4)_3$ Cathode Material Synthesized by a Sol-gel Method. *Electrochim. Acta* **52**, 5251-5257, doi:10.1016/j.electacta.2007.02.039 (2007).

43 Wurm, C., Morcrette, M., Rousse, G., Dupont, L. & Masquelier, C. Lithium Insertion/Extraction into/from $LiMX_2O_7$ Compositions (M = Fe, V; X = P, As) Prepared via a Solution Method. *Chem. Mat.* **14**, 2701-2710, doi:10.1021/cm020168e (2002).

44 Jiang, T. *et al.* Effects of Synthetic Route on the Structural, Physical and Electrochemical Properties of $Li_3V_2(PO_4)_3$ Cathode Materials. *Solid State Ion.* **180**, 708-714, doi:10.1016/j.ssi.2009.02.027 (2009).

Conference presentations without papers: 5

1. **Poster presentation** on "Electrochemical properties, valence state and local structure of α-Li3V2(PO4)3" by P.Balaya, Lee H.S., K. Saravanan, N.M. Suleimanov, D.R. Abdullin, P.N. Togulev (in collaboration with Zavoisky Physical Technical Institute of Russian Academy of Sciences, 420029, Kazan, Russian Federation), LIBD, Arcachon June 16-21, 2013.
2. **Invited talk** on "Role of Nanotechnology for Large Scale Energy Storage Systems" by Palani Balaya, International Conference on Nano Science & Engineering Applications, JNTU, Hyderabad, India June 26-28, 2014.
3. **Invited talk** on "High Rate Performing Li-ion Batteries for Military Applications", US-Singapore Power & Energy Workshop, Mark Center, Alexandria, VA, USA, 13-15 Nov. 2012
4. **Co-chair** of Symposium "Energy Harvesting and Storage: Materials, Devices and Applications – IV" at SPIE Conference on Defence Sensing and Security, 29 April to 3 May, 2013, Baltimore, Maryland, United States
5. **Co-chair** of Symposium "Energy Harvesting and Storage: Materials, Devices, and Applications V" at SPIE Conference on Defence Sensing and Security, Baltimore, USA, 5-9 May 2014.

Manuscripts submitted but not yet published: 1

1. "Nanostructured Mesoporous α-Li3V2(PO4)3/C for High Rate Lithium-ion Battery Applications", Lee Hwang Sheng, Nail Suleimanov, Vishwanathan Ramar, Mangayarkarasi Murugan, Kuppan Saravanan and Palani Balaya (**Manuscript in preparation** for submission to J. Phys. Chem. C)